Optical Materials 169 (2026) 117574

Contents lists available at ScienceDirect

Optical Materials

journal homepage: www.elsevier.com/locate/optmat

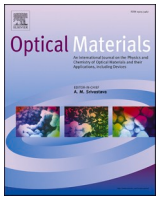

Research Article

Er^{3+}-doped BaY_2F_8 for non-contact lifetime thermometry: Combined effects of dopant concentration and programmable UV LED excitation

Danilo D. Tannus [a,b,c,*], Adriano B. Andrade [a,b], Giordano F.C. Bispo [e], Sonia L. Baldochi [d], Zélia S. Macedo [a,b], Mário E.G. Valerio [a,b]

[a] Materials Science and Engineering Graduate Course, Federal University of Sergipe, São Cristóvão, SE, 49107-230, Brazil
[b] Laboratory of Preparation and Characterization of Materials, Physics Department, Federal University of Sergipe, São Cristóvão, SE, 49107-230, Brazil
[c] Electrotechnical Coordination, Federal Institute of Sergipe, Campus Estância, SE, 49200-000, Brazil
[d] Center for Laser and Applications, IPEN/CNEN-SP, 11049, São Paulo, SP, 05422-970, Brazil
[e] Brazilian Synchrotron Light Laboratory (LNLS), Brazilian Center for Research on Energy and Materials (CNPEM), PO Box 6192, Campinas, SP 13083-970, Brazil

ARTICLE INFO

Keywords:
Luminescence
Lifetime
Optical thermometry
Fluorides
Erbium
Electronic module

ABSTRACT

This work presents a luminescence thermometry system based on a programmable electronic module designed for precise control of excitation pulses using a UV LED source, enabling time-resolved measurements of luminescence lifetime. This system was applied to investigate the influence of dopant concentration on the luminescence lifetime of Er^{3+} ions in a barium and yttrium fluoride matrix (BaY_2F_8) doped with different concentrations (1, 2, and 3 mol%) and their possible effects on thermometric usage. Spectroscopic measurements revealed that the sample with 3 mol% of Er^{3+} exhibited the highest luminescence efficiency, without evidence of concentration quenching. The luminescence lifetime decreased with increasing temperature, which was attributed to the increase in nonradiative de-excitation processes observed for all samples. The relative thermal sensitivity (S_r) was obtained from the lifetime dependence on temperature with the 3 mol% Er^{3+}-doped sample presenting the highest S_r, reaching 0.36 % K^{-1} at 317 K, indicating its potential usage as a non-contact luminescent thermometer. The measurements were performed via an electronic module specifically developed for excitation and lifetime-based luminescence detection, allowing precise control of the excitation pulse parameters. The repeatability of the measurements reached approximately 98 %, confirming that the sensor is stable and highly reproducible. The results demonstrate that lifetime-based luminescence thermometry using Er^{3+}-doped BaY_2F_8, combined with a programmable electronic module for precise excitation and detection control, provides a robust and accessible approach for temperature sensing, reducing the dependence on complex excitation sources, such as lasers, and increasing flexibility in data acquisition.

1. Introduction

The demand for increasingly accurate temperature measurements has driven the development of new approaches in thermometry. Among these methods, optical detection has emerged as an attractive approach because of its ability to perform noncontact measurements, enabling applications in systems where conventional sensors are rather unfeasible or may interfere with the process under evaluation. Several methodologies stand out among the luminescent thermometry techniques such as: the luminescence intensity ratio (LIR), emission peak band shift, bandwidth variation, and luminescence lifetime decay. For each one a specific characteristic is offered in terms of sensitivity and applicability.

Until recently, most of the works in luminescent thermometry have focused on luminescence intensity methodologies, and fewer studies have investigated the kinetic characteristics of luminescence. Luminescence lifetime-based thermometry overcomes some of the limitations associated with other techniques that rely on different spectroscopic parameters for temperature measurement. Although widely used, luminescence intensity ratio thermometry (LIR) presents drawbacks such as reduced thermal resolution and a low signal-to-noise ratio in weak emissions [1]. Moreover, the use of spectral parameters, such as emission peak band shifts and bandwidth broadening, also presents significant limitations, such as the need for high-resolution detection systems to accurately determine the peak position or the Full Width at

* Corresponding author. Materials Science and Engineering Graduate Course, Federal University of Sergipe, São Cristóvão, SE, 49107-230, Brazil.
E-mail address: danilodias13@gmail.com (D.D. Tannus).

https://doi.org/10.1016/j.optmat.2025.117574
Received 9 June 2025; Received in revised form 15 September 2025; Accepted 29 September 2025
Available online 30 September 2025

Half Maximum (FWHM) in real experimental conditions [2].

Early studies on lanthanide-activated phosphors indicated that temperature-induced variations in band shifts and bandwidth parameters are often too small to enable accurate measurements [3] because of the inherently narrow f–f transitions characteristic of these materials. In this context, lifetime-based thermometry has been proposed as an alternative to luminescent intensity thermometry methodologies. The main advantage of this technique is that luminescent decay is not affected by self-absorption or light scattering, making high-resolution measurements different from those of luminescent intensity-based methods [4]. Furthermore, measurements using lifetime-based thermometers are not affected by tissue depth in biological applications [5].

Different materials have been studied for luminescent thermometer applications, and the vast majority used LIR, such as Y_2O_3 [6], YF_3 [7], $NaYF_4$ [8], $NaY(MoO_4)_2$ [9], $Y_3Al_5O_{12}$ [10], YVO_4 [11], $CaBa_2WO_6$ [12], and among others. Over the past few years, the lifetime parameter has been increasingly used as a sensor for luminescent thermometry. Eu^{3+} and Sm^{3+}-doped $YNbO_4$ phosphor powders [13] were synthesized via solid-state reaction and evaluated as optical thermometers using both fluorescence intensity ratio (FIR) and luminescence lifetime methods. The lifetime curves showed clear thermal dependence from 303 K to 773 K and were well described by a temperature-dependent charge transfer (TDCT) model. Absolute sensitivities reached up to 7×10^{-3} K^{-1} at high temperatures, highlighting lifetime as an effective parameter for optical thermometry in harsh environments. Y_2O_3 nanoparticles co-doped with Yb^{3+}/Er^{3+} [14] were investigated as luminescent thermometers for biological applications, using upconversion luminescence and lifetime-based analysis. Suspended in aqueous medium, they exhibited a relative sensitivity of up to 0.50 % K^{-1} at 310 K, with lifetime measurements showing high stability and accuracy even under optical scattering conditions, reinforcing their potential for non-invasive in vivo thermal monitoring. (Sr,Ba)YTaO phosphors doped with Eu^{3+} [15] were synthesized via solid-state reaction and evaluated through lifetime-based luminescent thermometry, exhibiting high thermal stability and quantum yield. PDMS films doped with these phosphors showed promising performance for dual-function applications such as thermal sensing and anti-counterfeiting, highlighting the versatility of Eu^{3+}-based materials in optical technologies. Eu^{3+}-based metal–organic frameworks (MOFs) with multipodal benzoate ligands [16] were synthesized and evaluated as optical thermometers through fluorescence lifetime measurements. These structures exhibited strong luminescence, prolonged lifetimes, and high thermal and chemical stability, enabling a direct correlation between temperature and lifetime without the need for auxiliary ligands. The results highlight the strong potential of these MOFs for fluorescence-based sensing and the development of new rare-earth optical materials. Several other studies on luminescent thermometry can be found in the reviews [17,18].

Most of the system quoted herein and fund in the literature are yttrium-based materials due to the ability to replace Y host ions by rare-earth ions without charge compensation mechanisms and small lattice distortions. The advantage of using rare-earth ions in luminescent thermometry is their wide range of energy levels and intense luminescent emission [15]. The wide variety of electronic transitions in rare-earth ions gives rise to distinct decay time constants over a broad temporal range (nanoseconds to microseconds). These luminescent decays are affected by the physical properties of the sample as well as by the temperature and that is the main reason why they may be useful as a temperature probe [19].

Fluoride materials are particularly interesting in luminescent thermometry applications because of their high thermochemical and physical stability [20], low phonon energy [21], wide band gap [22], and high thermal conductivity [23]. Among others, barium yttrium fluoride (BaY_2F_8) has also been well studied as a potential material for luminescent thermometry applications [24–27]. However, all these reports are focused on luminescence intensity methodologies, such as the FIR and LIR, and there are no studies on lifetime-based thermometry properties in BaY_2F_8 to date. In this work, we explored the thermometric properties of Er^{3+}-doped BaY_2F_8 single-crystal samples [28]. Optical properties, with an emphasis on luminescence lifetime-based thermometry, were investigated in the range of 303–423 K. Measurements were carried out at different temperatures, allowing the influence of the doping concentration on the luminescent response of the material to be assessed. Additionally, structural and spectroscopic characteristics such as emission and excitation spectra were also discussed, providing complementary information on the luminescence processes in the Er-doped BaY_2F_8 system and its potential applicability as optical thermal sensors.

2. Methodology

Er^{3+}-doped BaY_2F_8 single crystals were grown via the zone melting method under a HF atmosphere from BaF_2 and YF^3 (and ErF_3) powders. The raw materials were weighed and mixed in a nonstoichiometric composition, according to the BaF_2-YF_3 phase diagram [29], with the addition of ErF_3 for doped samples with 1.0, 2.0 and 3.0 mol% nominal concentrations. The precursors were melted at 980 °C in a platinum reactor under HF flow, and Pt crucibles were used to prevent contamination. Subsequently, Er^{3+}-doped BaY_2F_8 single crystals were grown via the floating zone (FZ) melting method under a HF atmosphere, resulting in ingot crystals with high purity. The zone melting method enables crystal growth by moving a localized molten region along a solid material, allowing controlled solidification and redistribution of impurities due to solubility differences between the solid and liquid phases [30].

The grown crystals exhibited an ingot-like morphology, with a transparent monocrystalline central region. An example of the central region of the 2 mol% Er-doped BaY_2F_8 crystal is shown in the supplementary material on Fig. S1. Crystals of approximately 4 cm in length were obtained, free of cracks, inclusions, and bubbles. More detailed information on the crystal growth procedure, and sets of Scanning Electron Microscopy (SEM) images of the samples can be seen in detail in Cruz [30]. The single crystals were powdered by grinding in an agate mortar and used for characterization.

The crystalline structure of the samples was investigated via X-ray diffraction (XRD), which was carried out in a RIGAKU Ultima+ 2000/PC diffractometer with Cu Kα radiation. The measurement was performed at room temperature and atmospheric pressure, operating at 40 kV/30 mA, with a 2θ range from 20° to 65° in step scan mode with steps of 0.02°. The experimental data were compared with the powder XRD pattern of the standard crystal structure extracted from the Inorganic Crystal Structure Database (ICSD).

The excitation and emission spectra were recorded for all Er-doped BaY_2F_8 sample (1, 2 and 3 mol%), using an ISS PC1 spectrofluorometer using an ENERGETIQ plasma lamp (model EQ-99) and an excitation monochromator operating in the 180–800 nm range, with a spectral resolution of 0.25 nm. Excitation spectra were acquired with the emission fixed at 550 nm, whereas emission spectra were obtained with the excitation fixed at 378 nm, using a 470 nm high-pass filter and an Ocean Optics QE65 Pro spectrometer coupled to the fluorimeter via an optical fiber.

Luminescence lifetime measurements were performed by exciting Er^{3+}-doped samples via an ultraviolet (UV) LED with an emission peak centered at 390 nm, driven by an electronic module specifically designed to excite photoluminescent materials via voltage signals adjustable via pulse width modulation (PWM) [31]. The module allows the adjustment of the time interval during which the excitation LED remains on (T_{ON}), i.e., the sample excitation period, and the interval in which the LED remains off (T_{OFF}), corresponding to the decay curve acquisition time. These intervals can be set from milliseconds down to hundreds of nanoseconds, offering an efficient and affordable solution for time-resolved luminescence studies across a wide range of materials.

In addition to the electronic circuit, a graphical interface was developed to control and monitor the excitation parameters in a user-friendly way. This interface enables real-time configuration of T_{ON} and

T_{OFF} values and selection of the time unit (ms, μs, or ns), allowing flexible adaptation to different experimental conditions and emission decay profiles. The system was designed to be portable, low-cost, and compatible with commercial LEDs, eliminating the need for pulsed laser systems excitation. A patent related to this device has been filed (BR 10 2025 009260 3), and its architecture and operation were essential to enable precise control over the excitation cycles used throughout this study. An example of the interface and excitation waveform is provided in the Supplementary Information (Fig. S2).

Fig. S3 shows the schematic setup used in the luminescence decay time measurements, which were carried out with a JANIS CCS-450 cryostat system as the sample holder and included a CTI-CRYOGENICS model 8200 closed-cycle helium compressor and a REFRISAT water chiller unit. A LAKESHORE 340 temperature controller (a) was employed, along with the sample chamber (b), where the sample under analysis was placed and all the required components for the measurements were integrated, including the excitation LED (c) and a HAMAMATSU photomultiplier tube, model PMT R928 (d), powered with a stabilized high-voltage supply, and model TCH 3000-2XA1A from TECTROL (e). The PMT signal was visualized via an oscilloscope model LECROY WAVESURFER 104 (f). The same setup was used to measure the signal from the excitation LED itself, which was reflected off the rear side of an aluminum sample holder to obtain the pulse profile. All measurements were performed in triplicate, using an excitation pulse of 1 ms (T_{ON}) followed by 4 ms (T_{OFF}), programmed by the electronic module (g), over a temperature range from 303 K to 423 K in steps of 10 K. The full setup used for lifetime measurements is illustrated in Fig. S3.

3. Results and discussion

Fig. 1 shows the XRD patterns of the undoped and doped samples compared with the reference pattern [32]. No additional diffraction peaks were observed for the Er^{3+}-doped samples, which indicates that no additional phases were formed by the presence of the dopant and since Er has a lower vapour pressure than either Ba or Y [33], this is a strong indication that the dopant ions were successfully incorporated into the host matrix.

Photoluminescence (PL) measurements were performed to investigate the Er^{3+} electronic transitions in the BaY_2F_8 host and to investigate the influence of different dopant concentrations on the intensity and spectral distribution of the light emitted by the samples. Figs. 2 and 3 show the excitation and emission spectra, respectively, for all samples. In the excitation spectrum (Fig. 2), all samples exhibit well-defined peaks in the 350–425 nm region, attributed to the characteristic electronic transitions of Er^{3+}, with the main excitation peak centered at 378 nm. The spectral shape is similar for all samples with different dopant concentrations suggesting that the electronic structure of the emitting centres remains unchanged. However, the relative peak intensities vary with the Er^{3+} concentration, being highest for the sample with 3 mol% Er-doped (blue line). This increase is clearly associated with higher photon absorption due to the higher density of active ions, resulting in a more intense optical response. The following electronic transitions could be identified in the excitation spectrum: $^4I_{15/2} \rightarrow {}^2K_{15/2}$, $^4I_{15/2} \rightarrow {}^4G_{9/2}$, $^4I_{15/2} \rightarrow {}^4G_{11/2}$ (most intense peak), and $^4I_{15/2} \rightarrow {}^2G_{9/2}$ [34,35].

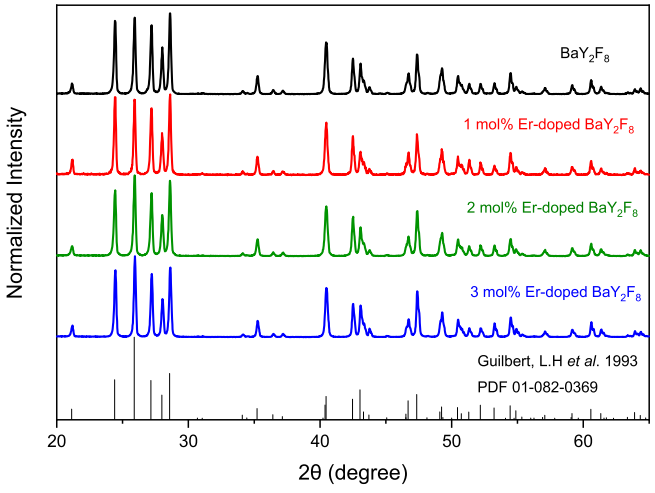

Fig. 1. X-ray diffraction measurements of undoped and Er-doped BaY_2F_8.

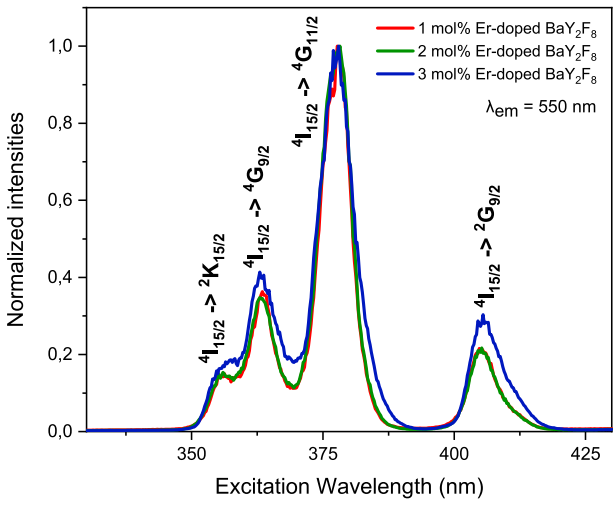

Fig. 2. Excitation spectrum of Er-doped BaY_2F_8 samples with different Er concentrations.

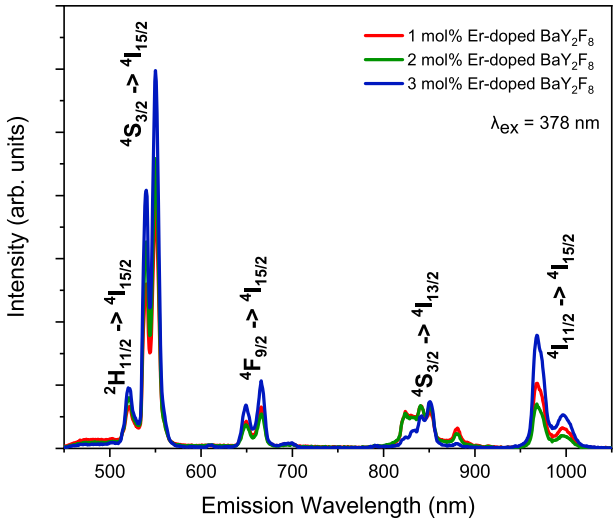

Fig. 3. Emission spectrum of Er-doped BaY_2F_8 samples with different Er concentrations.

Fig. 3 shows the emission spectra for all samples obtained under 378 nm excitation. It reveals multiple characteristic Er^{3+} peaks in the 500–1100 nm range, with green emission corresponding to the $^2H_{11/2} \rightarrow {}^4I_{15/2}$ and $^4S_{3/2} \rightarrow {}^4I_{15/2}$ transitions (most intense peak), red emission corresponding to $^4F_{9/2} \rightarrow {}^4I_{15/2}$, and other transitions such as $^4S_{3/2} \rightarrow {}^4I_{13/2}$ and $^4I_{11/2} \rightarrow {}^4I_{15/2}$ [22,34–36]. The emission band intensities follow the same trend observed in the excitation spectra, being highest for the 3 mol% Er-doped sample. This behaviour suggests that, up to this concentration, increasing the dopant still enhances the luminescence intensity, with no clear evidence of concentration quenching.

Luminescence lifetime measurements were performed in triplicate for the three samples. The time decay curves were measured separately

and the luminescence lifetime values were obtained from fitting the experimental curves to a first order single exponential decay model and the values obtained can be seen in the supplementary material on Tables S1, S2, and S3, showing the calculated lifetime values, the fitting errors and χ^2 of the fittings, average lifetime, and standard deviation, considering the entire proven temperature range. Also in the supplementary material, Fig. S4 presents triplicate measurements of the sample 2 mol% Er^{3+}-doped measured at two chosen temperatures, 303 and 423 K. It can be seen that the independent measurements displayed quite small variations in the same temperatures. Further discussions in this work consider only the average lifetime of the three independent measurements performed for each sample at each temperature.

Fig. 4 shows the average luminescence decay time measurements for all the samples. The measurements were performed with temperatures varying from 303 K to 423 K in 10 K intervals, for the Er^{3+}-doped samples with 1.0 (b), 2.0 (c) and 3.0 mol% (d). Fig. 4 (a) shows the curve fitted considering exponential-type decay, and the fitting was performed considering that the experimental response is a result of the true luminescence decay response of the sample convoluted to the excitation profile (also indicated in Fig. 4(a)). The fittings were done via the ISS Vinci software package that basically search the best set of parameters of the first order decay exponential model that convoluted to the measured experimental excitation profile reproduces the response curves. It is important to mention that the excitation pulse width was fixed at 1 ms, a value selected to ensure that the system reached a steady-state excitation regime prior to the decay acquisition [37,38]. This condition was verified experimentally based on the growth profile of the signals and lifetime values under excitation with pulses from 50 μs to 2 ms, as shown in Fig. S5, indicating that the T_{ON} of 1 ms was the smallest value considered that indicates that a steady state under excitation is achieved.

The measurements revealed a decrease in the component with increasing temperature which can be attributed to increases in nonradiative deexcitation processes, such as energy transfer between neighbouring Er^{3+} ions assisted by phonons [24]. As the temperature increases, the lattice vibrations intensify, favouring nonradiative energy transfer and consequently reducing the luminescence efficiency. As a result, the luminescence lifetime decreases, making it possible to establish a correspondence between the luminescence lifetime and the temperature. In this model, the radiative rate is considered constant, as it does not influence the decay time with temperature variation. Considering a two-level system composed of a ground state and an excited state, the luminescence lifetime (τ) as a function of temperature is given by:

$$\tau(T) = \frac{1}{k_R + k_{NR}(T)} \tag{1}$$

where $k_R = 1/\tau_R$ is the radiative transition rate, $k_{NR}(T) = 1/\tau_{NR}(T)$ is the nonradiative transition rate, τ_R is the radiative lifetime, and $\tau_{NR}(T)$ is the nonradiative lifetime.

According to the Mott–Seitz (MS) model [39], the nonradiative transition rate varies with temperature as follows:

$$k_{NR}(T) = k_{NR0} e^{\left(\frac{-\Delta E}{kT}\right)} \tag{2}$$

where k_{NR0} is the nonradiative transition rate at zero K, ΔE is the activation energy of the nonradiative process or the energy gap between the excited and lower levels, and k is the Boltzmann constant. By multiplying Eq. (1) by the radiative lifetime, which is denoted as τ_0 since it is constant in this case, and relating it to Eq. (2), the luminescence lifetime as a function of temperature in the MS model can be expressed as:

$$\tau(T) = \frac{\tau_0}{1 + \tau_0 k_{NR0} e^{\left(\frac{-\Delta E}{kT}\right)}} \tag{3}$$

Fig. 5 presents the lifetime values obtained over the temperature range from 303 K to 423 K, along with the curve fittings using the MS model. The τ vs. T data for all the samples exhibit a decreasing trend

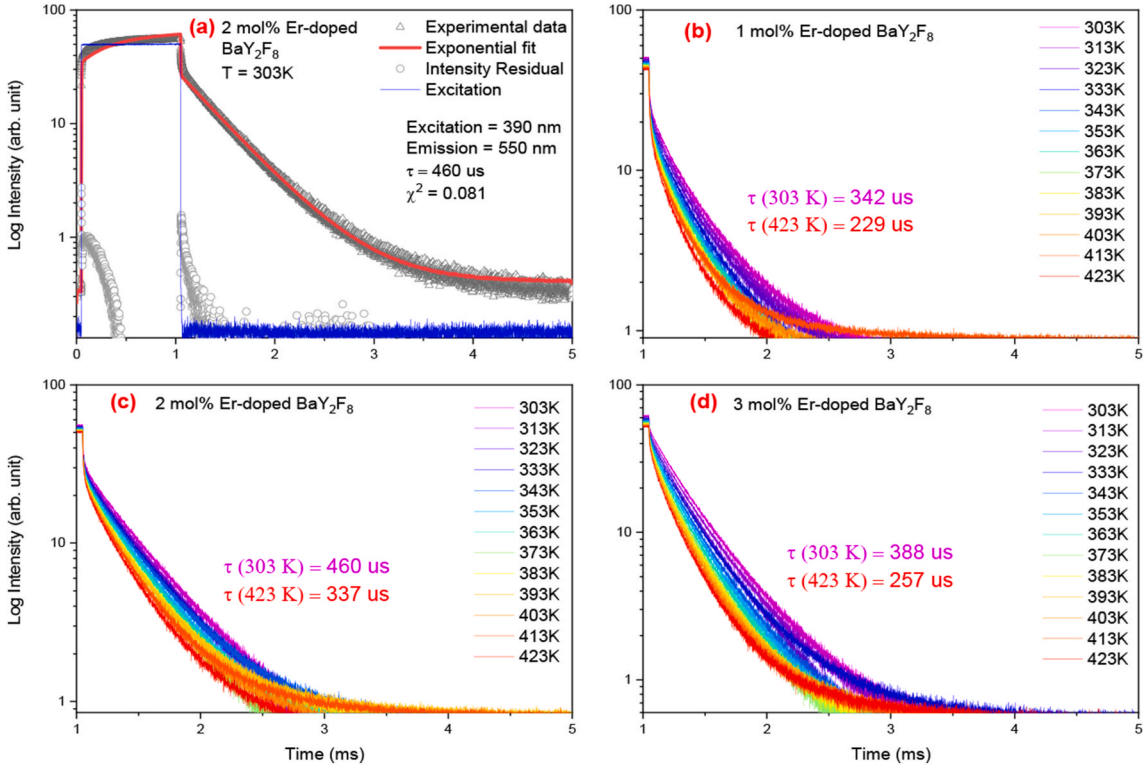

Fig. 4. Luminescence lifetime decay curves: experimental data, exponential fit, residual intensity and excitation signal of 2 mol% Er-doped BaY_2F_8 at 303 K (a), 1 mol% Er-doped BaY_2F_8 from 303 K to 423 K (b), 2 mol% Er-doped BaY_2F_8 from 303 K to 423 K (c) and 3 mol% Er-doped BaY_2F_8 from 303 K to 423 K (d).

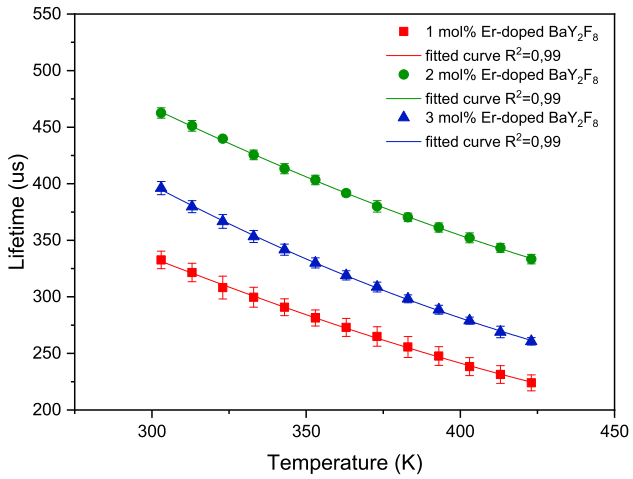

Fig. 5. Dependence of the luminescence lifetimes with temperature from 303 K to 423 K and corresponding fitted curves for all Er-doped BaY_2F_8 samples.

with increasing temperature. The fitting results are in good agreement with the experimental data. This behaviour is characteristic of thermally activated de-excitation processes in which the increase in temperature enhances the interaction between Er^{3+} ions and phonons in the crystal lattice, favouring nonradiative relaxation mechanisms as proposed by Shi and Mudring [40]. In the 3 mol% Er^{3+}-doped sample, although the emission is more intense (Fig. 3), the lifetime is shorter than that of the 2 mol% Er^{3+}-doped sample, suggesting that interactions between dopant ions can promote nonradiative energy transfer processes, reducing the persistence of luminescence. Thus, although concentration quenching does not yet dominate the luminescence emission efficiency of the 3 mol % Er^{3+}-doped sample, the lifetimes indicate that ion–ion interactions may be already in place affecting the relaxation dynamics, shortening the decay time of the highly doped sample.

Using the results from Fig. 5, it is possible to calculate the relative sensitivity (S_r). This parameter is the absolute sensitivity normalized to the measured quantity, i.e., the percentage variation of the variable being measure as function of T per unit of temperature change (%K^{-1}), as shown in equation (4). Relative sensitivity allows for the comparison of different thermometric methods, such as those based on the intensity ratio and luminescence lifetime.

$$S_r = \frac{S_a}{\tau}100\% = \frac{1}{\tau}\left|\frac{d\tau}{dT}\right|100\% \quad (4)$$

Fig. 6 shows the results of the calculated relative sensitivity (S_r) for

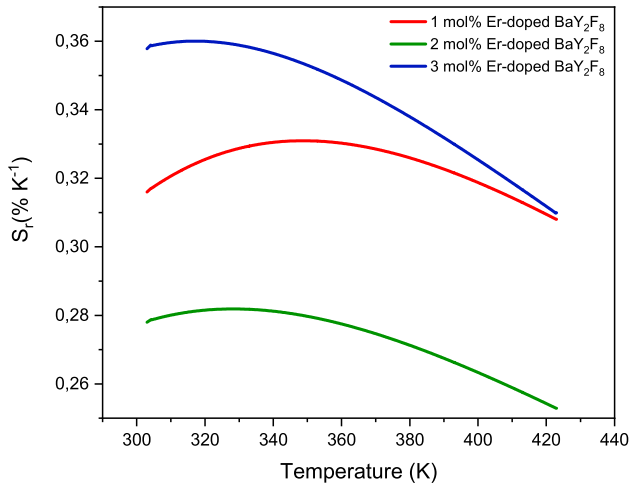

Fig. 6. Relative sensitivity of Er-doped BaY_2F_8 samples from 303 K to 423 K.

all three concentrations of Er^{3+} showing that the 3 mol% Er^{3+}-doped sample (blue curve) presented the highest S_r across the entire analysed temperature range, with a maximum of 0.36 % K^{-1} at 317 K, indicating that this sample is the most suitable for luminescent thermometry applications within the screened dopant concentration. This means that it can provide better performance as a thermal sensor, allowing higher resolution when considering different temperatures, since it shows a more significant variation in lifetime as temperature changes. Furthermore, the temperature resolution (or temperature uncertainty) was estimated using the expression:

$$\delta T = \frac{1}{S_R}\cdot\frac{\delta\tau}{\tau} \quad (5)$$

where the relative thermometric parameter error is defined as $\delta\tau/\tau$. For the 3 mol% Er-doped BaY_2F_8 sample, which presented the best thermometric performance among the investigated compositions, the minimum thermal resolution achieved was 0.034 K at 403 K. Thermal resolution values below than 0.1 K are considered satisfactory [41]. Thus, the system studied in the work meets this criterion in the investigated range. The full resolution profiles for all samples over the 303–423 K range are presented in the Supplementary material (Fig. S6). As shown in the Supplementary material on Table S2 and S3, both the 2 mol% Er^{3+}-doped and 3 mol% Er^{3+} -doped samples exhibit consistent statistical behaviour, with low standard deviations and strong agreement among the triplicate lifetime measurements. Notably, the 3 mol% Er^{3+}-doped sample not only displays the highest sensitivity among the compositions but also a more pronounced lifetime decreases with increasing temperature. This is accompanied by high reproducibility, lower uncertainty at most temperature points, and robust lifetime stability across repeated measurements, supporting its suitability for accurate and reliable thermal sensing applications.

Table 1 presents the relative sensitivity (S_r) values for Er^{3+} dopants in different host matrices, as reported in the literature. For comparison purposes, only the maximum S_r value within the 303–423 K temperature range was considered for each case. The analysis includes various luminescence-based methodologies, such as the fluorescence intensity ratio (FIR), bandwidth, band shift and lifetime. The values obtained in the present study are comparable to those reported for other matrices.

Although the S_r determined here is not among the highest reported, the lifetime-based approach offers significant advantages, such as independence from excitation uniformity and sample geometry and reduced susceptibility to external influencing factors that can compromise measurements in other methodologies. However, one limitation of this technique is the requirement that the excitation pulse width and time between pulses of the light source must match the timescale of the

Table 1
Performance comparison of thermal sensors based on different luminescence methods using Er^{3+} dopants in various host matrices (with the maximum S_r value considered within the 303–423 K temperature range).

Material	Exc. (nm)	Method	S_r (% K^{-1})	Ref.
PbNa	810	FIR	0,31	[46]
PbW	810	FIR	0,2	[46]
$CaBa_2WO_6$	980	FIR	0,45	[12]
$Ba_4Yb_3F_{17}$	980	FIR	0,2	[47]
YOF	365	FIR	1,67	[48]
$BaGd_2O_4$	377	FIR	1,6	[49]
$NaLaMgWO_6$	378	FIR	1,04	[50]
La_2MgTiO_6	380	FIR	1107	[51]
$Na_5Gd_9F_{32}$	980	FIR	1,08	[52]
YVO_4	350	Bandwidth	0,35	[11]
YVO_4	350	Band shift	0,34	[11]
$Cs_3GdGe_3O_9$	980	Lifetime	0,49	[44]
$NaYF_4$	980	Lifetime	0,16	[45]
$Cs_2(Na/Ag)BiCl_6$	980	Lifetime	0,38	[42]
Y_2O_3	522	Lifetime	0,37	[43]
BaY_2F_8	**390**	**Lifetime**	**0,36**	**This work**

analysed material. One of the novelty results of the present work, in addition to study of the usage of the luminescence lifetime of Er-doped BaY_2F_8 as a potential contactless thermometry was the development of electronic module [31] which was required and used to measure the luminescence lifetime, allowing precise programming of the excitation exposure time duration (T_{ON}) and the interval between light pulses (T_{OFF}) of the light source. Furthermore, the use of LEDs as the excitation source makes the experimental setup more accessible than systems that employ lasers, as is the case in most of the studies listed in Table 1, particularly the LIR methodology-based ones and those that also use the lifetime-based approach [42–45], among other recent studies.

To evaluate the signal reproducibility and stability of the thermometric sensing, ten consecutive cycles of heating–cooling of the material were performed. At each cycle, the lifetime at minimum and maximum temperatures was measured for the 3 mol% Er^{3+}-doped sample since it presented the best relative sensitivity. The results of these cycles are shown in Fig. 7 and the repeatability were quantified via equation (6) [53]:where Δ_m is the average value of the temperature measurement parameter and Δ_i corresponds to the individual value of the measured parameter in each cycle. Good repeatability is indicated when $R > 95$ % [54]. The results obtained here confirm the high chemical stability of inorganic fluoride matrices [7], demonstrating the excellent performance of the luminescence lifetime-based thermometer, with approximately 98 % repeatability.

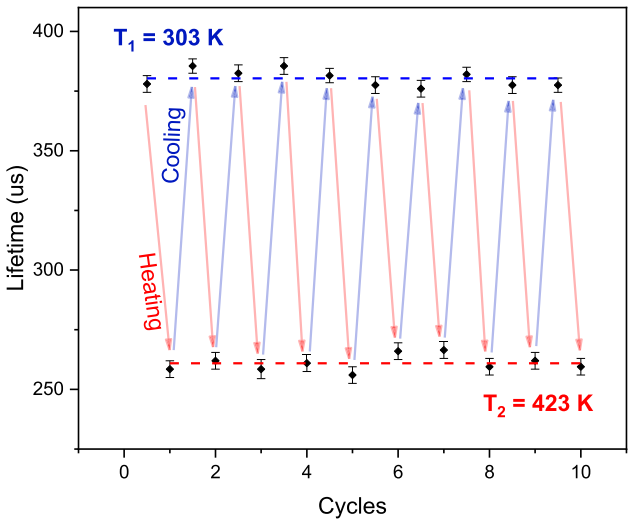

Fig. 7. Repeatability cycles in the 303–423 K temperature range.

$$R = \left(1 - \frac{\max(|\Delta_m - \Delta_i|)}{\Delta_m}\right) x100\% \quad (6)$$

4. Conclusion

This study evaluated the performance of Er^{3+}-doped BaY_2F_8, with concentrations of 1, 2, and 3 mol%, as a thermal sensor based on the luminescence lifetime. The excitation and emission spectra indicated that the 3 mol% Er^{3+}-doped sample presented the highest luminescence overall efficiency, whereas the lifetime analysis revealed a decreasing trend with increasing temperature, confirming the intensification of nonradiative processes. Although increasing the dopant concentration to 3 mol% did not cause noticeable quenching of the luminescence efficiency, energy interactions between dopant ions began to influence the de-excitation processes, resulting in a reduced luminescence lifetime.

The temperature dependence of the relative sensitivity (S_r) revealed that the 3 mol% Er^{3+}-doped sample was the most sensitive one reaching a value of $S_r = 0.36$ % K^{-1} at 317 K and, as a consequence, is the best sample within this work for contactless luminescence thermometric applications. Additionally, the repeatability measurements for this sample also demonstrated high reproducibility with approximately 98 %, further reinforcing the feasibility of the material for practical applications. Compared with other Er^{3+}-based luminescent thermometers, the lifetime-based method offers significant advantages, such as independence from the excitation source intensity and reduced susceptibility to geometric and environmental variations.

Finally, compared to recent related studies, this work contributes to the field by introducing Er^{3+}-doped BaY_2F_8 as a novel material with potential application as lifetime-based luminescent thermometry. Another important output of the present work was the development of a suitable and programmable electronic module specifically for lifetime measurements, which allowed precise adjustments of the time profile, or duty cycle, of the excitation source with variable T_{ON} and T_{OFF} parameters. Combined with the use of commercial LED's, this module allowed a precise experimental control, reducing costs, as compared to the laser-based systems. Thus, the results of this study not only contribute to the understanding of the thermal luminescence mechanisms in Er^{3+}-doped BaY_2F_8 but also reinforce its applicability as a promising material for optical thermal sensing with a relatively easy and cost-effective setup.

CRediT authorship contribution statement

Danilo D. Tannus: Writing – original draft, Validation, Methodology, Investigation, Formal analysis, Data curation, Conceptualization. **Adriano B. Andrade:** Writing – review & editing, Validation, Supervision, Conceptualization. **Giordano F.C. Bispo:** Writing – review & editing, Conceptualization. **Sonia L. Baldochi:** Writing – review & editing. **Zélia S. Macedo:** Writing – review & editing, Funding acquisition. **Mário E.G. Valerio:** Writing – review & editing, Supervision, Project administration, Funding acquisition.

Declaration of competing interest

The authors declare that they have no known competing financial interests or personal relationships that could have appeared to influence the work reported in this paper.

Acknowledgments

The authors acknowledge CNPq and CAPES (Brazil) for financial support, AGITTE/UFS for support through the PICSrev No. 28/2024 and Minha Patente No. 21/2024 programs. Danilo D. Tannus grateful thanks to CAPES for the scholarship (88887.950888/2024–00), CNPq (141937/2025-4) and Mário E.G. Valerio thanks to CNPq (grants 317283/2021-9).

Appendix A. Supplementary data

Supplementary data to this article can be found online at https://doi.org/10.1016/j.optmat.2025.117574.

Data availability

Data will be made available on request.

References

[1] L. Cui, Z. Dong, D. Yu, Y. Wang, e A. Meijerink, High-sensitivity luminescent temperature sensors: MFX:1%Sm^{2+} (M = Sr, Ba, X = Cl, Br), Sci. Adv. 10 (33) (2024) eado7737, https://doi.org/10.1126/sciadv.ado7737, ago.

[2] I.E. Kolesnikov, et al., YVO4:Nd3+ nanophosphors as NIR-to-NIR thermal sensors in wide temperature range, Sci. Rep. 7 (1) (2017) 18002, https://doi.org/10.1038/s41598-017-18295-w dez.

[3] M.D. Dramićanin, Trends in luminescence thermometry, J. Appl. Phys. 128 (4) (jul. 2020) 040902, https://doi.org/10.1063/5.0014825.

[4] X. Su, et al., Lifetime-based nanothermometry *in vivo* with ultra-long-lived luminescence, Chem. Commun. 56 (73) (2020) 10694–10697, https://doi.org/10.1039/D0CC04459H.

[5] T. Chihara, et al., Biological deep temperature imaging with fluorescence lifetime of rare-earth-doped ceramics particles in the second NIR biological window, Sci. Rep. 9 (1) (2019) 12806, https://doi.org/10.1038/s41598-019-49291-x set.

[6] M.A. Gomes, et al., Temperature-sensitive luminescence of Y2O3:Nd3+ nanocrystals produced by an eco-friendly route, Opt. Mater. 89 (mar. 2019) 536–542, https://doi.org/10.1016/j.optmat.2019.01.064.

[7] M.S. Pudovkin, A.K. Ginkel, e E.V. Lukinova, Temperature sensitivity of Nd3+, Yb3+:YF3 ratiometric luminescent thermometers at different Yb3+ concentration, Opt. Mater. 119 (2021) 111328, https://doi.org/10.1016/j.optmat.2021.111328 set.

[8] W. Zhou, J. Yang, X. Jin, Y. Peng, e J. Luo, A high-sensitivity optical thermometer based on Nd3+/Tm3+/Yb3+/Gd3+ four-doped NaYF4 nanomaterials, J. Lumin. 246 (jun. 2022) 118807, https://doi.org/10.1016/j.jlumin.2022.118807.

[9] D.L. Silva, R.S. Pugina, e J.M. Almeida Caiut, Green, red, and near-infrared up-conversion emission of NaY(MoO4)2:Er3+ submicrometric particles obtained by one-step synthesis, and its thermometric application, J. Lumin. 243 (mar. 2022) 118639, https://doi.org/10.1016/j.jlumin.2021.118639.

[10] D. Chen, S. Liu, Y. Zhou, Z. Wan, P. Huang, e Z. Ji, Dual-activator luminescence of RE/TM:$Y_3Al_5O_{12}$ (RE = Eu^{3+}, Tb^{3+}, Dy^{3+}; TM = Mn^{4+}, Cr^{3+}) phosphors for self-referencing optical thermometry, J. Mater. Chem. C 4 (38) (2016) 9044–9051, https://doi.org/10.1039/C6TC02934E.

[11] I.E. Kolesnikov, D.V. Mamonova, M.A. Kurochkin, E. Yu Kolesnikov, e E. Lähderanta, Multimode luminescence thermometry based on emission and excitation spectra, J. Lumin. 231 (mar. 2021) 117828, https://doi.org/10.1016/j.jlumin.2020.117828.

[12] J. Xu, Y. Bu, J. Wang, L. Meng, X. Wang, e X. Yan, Site-dependent photoluminescence and optical thermometric behaviors of double-perovskite CaBa2WO6:Er3+, Chem. Phys. Lett. 749 (jun. 2020) 137410 https://doi.org/10.1016/j.cplett.2020.137410.

[13] Lj R. Đačanin, S.R. Lukić-Petrović, D.M. Petrović, M.G. Nikolić, e M.D. Dramićanin, Temperature quenching of luminescence emission in Eu3+- and Sm3+-doped YNbO4 powders, J. Lumin. 151 (jul. 2014) 82–87, https://doi.org/10.1016/j.jlumin.2014.02.008.

[14] L.F. Dos Santos, et al., Lifetime-based luminescence thermometry from Yb3+/Er3+ codoped nanoparticles suspended in water, J. Lumin. 262 (2023) 119946, https://doi.org/10.1016/j.jlumin.2023.119946 out.

[15] Y. Hua, T. Wang, H. Li, J.S. Yu, e L. Li, Charge transfer band excited (Sr,Ba)2YTaO6:Eu3+ reddish-orange-emitting phosphors for luminescence lifetime thermometry and flexible anti-counterfeiting labels, J. Alloys Compd. 930 (jan. 2023) 167454, https://doi.org/10.1016/j.jallcom.2022.167454.

[16] C. Wang, P. Xi, W. Shi, X. Yan, C. Zhang, e B. Cheng, Structure, fluorescence enhancement mechanism and luminescence thermometry functions of multi-podal benzoate Eu(III) luminescent materials, Mater. Res. Bull. 192 (2025) 113627, https://doi.org/10.1016/j.materresbull.2025.113627 dez.

[17] L. Marciniak, K. Kniec, K. Elżbieciak-Piecka, K. Trejgis, J. Stefanska, e M. Dramićanin, Luminescence thermometry with transition metal ions. A review, Coord. Chem. Rev. 469 (2022) 214671–out, https://doi.org/10.1016/j.ccr.2022.214671.

[18] L. Đačanin, Far e M. Dramićanin, Luminescence thermometry with nanoparticles: a review, Nanomaterials 13 (21) (nov. 2023) 2904, https://doi.org/10.3390/nano13212904.

[19] S. Adachi, Review—Temperature dependence of transition-metal and rare-earth ion luminescence (Mn^{4+}, Cr^{3+}, Mn^{2+}, Eu^{2+}, Eu^{3+}, Tb^{3+}, etc.) II: Experimental Data Analyses, ECS J. Solid State Sci. Technol. 11 (10) (2022) 106002–out, https://doi.org/10.1149/2162-8777/ac91f5.

[20] E. Koch, Metal-Fluorocarbon Based Energetic Materials, first ed., Wiley, 2012 https://doi.org/10.1002/9783527644186.

[21] K. Trejgis, K. Ledwa, K. Maciejewska, L. Li, e L. Marciniak, Modulation of thermometric performance of single-band-ratiometric luminescent thermometers based on luminescence of Nd3+ activated tetrafluorides by size modification, Sci. Rep. 12 (1) (2022) 5847, https://doi.org/10.1038/s41598-022-09912-4, abr.

[22] A.B. Andrade, G.F. da C. Bispo, Z.S. Macedo, S.L. Baldochi, E.G. Yukihara, e M.E. G. Valerio, VUV excited luminescence and thermoluminescence investigation on Er3+- or Pr3+-doped BaY2F8 single crystals, Opt. Mater. 90 (abr. 2019) 238–243, https://doi.org/10.1016/j.optmat.2019.02.044.

[23] Y.-Y. Qi, T. Zhang, Y. Cheng, X.-R. Chen, D.-Q. Wei, e L.-C. Cai, Lattice dynamics and thermal conductivity of calcium fluoride via first-principles investigation, J. Appl. Phys. 119 (9) (mar. 2016) 095103, https://doi.org/10.1063/1.4942841.

[24] S. Wang, Y. Ruan, T. Tsuboi, H. Tong, Y. Wang, e S. Zhang, Temperature dependence of luminescence behavior in Er3+-doped BaY2F8 single crystal, Phys. B Condens. Matter 431 (dez. 2013) 37–43, https://doi.org/10.1016/j.physb.2013.08.046.

[25] Shuai Wang, Yongfeng Ruan, e Pengfei Wang, Investigation on thermal excitation mechanism of Er^(3+)-doped BaY_2F_8 single crystal, World Scient. Res. J. 7 (5) (2021), https://doi.org/10.6911/WSRJ.202105_7(5).0003 maio.

[26] G.B. Nair, A.K. Sharma, S.J. Dhoble, e H.C. Swart, Upconversion process in BaY_2F_8:Yb^{3+},Ho^{3+} phosphor for optical thermometry, Luminescence 36 (8) (2021) 1847–1850, https://doi.org/10.1002/bio.3923, dez.

[27] A.K. Sharma, G.B. Nair, S.J. Dhoble, R.E. Kroon, J.J. Terblans, e H.C. Swart, Luminescence thermometry based on the upconversion luminescence from the stark sublevels of BaY2F8:Yb3+, Tm3+ phosphor, J. Fluoresc. 34 (3) (maio 2024) 1039–1048, https://doi.org/10.1007/s10895-023-03295-z.

[28] A.C.S. De Mello, A.B. Andrade, G.H.G. Nakamura, S.L. Baldochi, e M.E. G. Valerio, Luminescence properties of Er3+ and Tm3+ doped BaY2F8, J. Lumin. 138 (jun. 2013) 19–24, https://doi.org/10.1016/j.jlumin.2012.12.001.

[29] G.H.G. Nakamura, S.L. Baldochi, V.L. Mazzocchi, C.B.R. Parente, M.E.G. Valério, e D. Klimm, Problems in the thermal investigation of the BaF2-YF3 system, J. Therm. Anal. Calorim. 95 (1) (jan. 2009) 43–48, https://doi.org/10.1007/s10973-008-9005-3.

[30] S.F. de A. Cruz, Crescimento e Caracterização de Monocristais de BaY2F8:TR onde TR = Nd3+, Pr3+, Er3+, Tb3+, Dy3+, Univ. São Paulo, 2008. Ph.D. Thesis, http://www.teses.usp.br/teses/disponiveis/85/85134/tde-13102011-103049/pt-br.php.

[31] M.E.G. Valerio, D.D. Tannus, A.B. Andrade, A.S. Silva, e Z.S. Macedo, Módulo de controle para excitação de materiais fotoluminescentes, BR 10 2025 009260 3 [Online]. Disponível em: https://revistas.inpi.gov.br/pdf/Patentes2837.pdf.

[32] L.H. Guilbert, J.Y. Gesland, A. Bulou, e R. Retoux, Structure and raman spectroscopy of czochralski-grown barium yttrium and barium ytterbium fluorides crystals, Mater. Res. Bull. 28 (9) (1993) 923–930, https://doi.org/10.1016/0025-5408(93)90039-G, set.

[33] David R. Lide (Ed.), CRC Handbook of Chemistry and Physics, 84th Edition, (National Institute of Standards and Technology). CRC Press LLC, Boca Raton, 2003, https://doi.org/10.1021/ja0336372, 2616 pp. $139.95. ISBN 0-8493-0484-9.," J. Am. Chem. Soc., vol. 126, n° 5, pp. 1586–1586, fev. 2004.

[34] A.M. Tkachuk, S.É. Ivanova, M.-F. Joubert, e Y. Guyot, Spectroscopic study of double sodium-yttrium fluoride crystals doped with erbium Na0.4Y0.6F2.2:Er3+: I. Intensities of luminescence spectra and kinetics of luminescence, Opt. Spectrosc. 97 (2) (2004) 251–269, https://doi.org/10.1134/1.1790643, ago.

[35] V.L. Paperny, et al., Enhancement of photoluminescence from rare-earth ions in fluoride crystals by ion-implanted silver nanoparticles, J. Lumin. 279 (2025) 121044, https://doi.org/10.1016/j.jlumin.2024.121044 abr.

[36] S. Bedamati, M. Behera, R. Arun Kumar, K. Shwetabh, e K. Kumar, Sodium yttrium fluoride doped with Er3+ ions for thermally and non-thermally coupled nano-thermometry and IR detection applications, J. Mol. Liq. 411 (2024) 125685–out, https://doi.org/10.1016/j.molliq.2024.125685.

[37] A. Casillas-Rubio, D. Mendez-Gonzalez, M. Laurenti, J. Rubio-Retama, O. G. Calderón, e S. Melle, Impact of excitation pulse width on the upconversion luminescence lifetime of $NaYF_4$:Yb^{3+} ,Er^{3+} nanoparticles, Nanoscale 16 (25) (2024) 12184–12195, https://doi.org/10.1039/D4NR00718B.

[38] L. Labrador-Páez, et al., Excitation pulse duration response of upconversion nanoparticles and its applications, J. Phys. Chem. Lett. 13 (48) (2022) 11208–11215, https://doi.org/10.1021/acs.jpclett.2c03037, dez.

[39] C.C. KLICK, e J.H. Schulman, Luminescence in solids, Solid State Phys. 5 (1957) 97–172.

[40] R. Shi, e A.-V. Mudring, Phonon-mediated nonradiative relaxation in Ln^{3+} -Doped luminescent nanocrystals, ACS Mater. Lett. 4 (10) (2022) 1882–1903, https://doi.org/10.1021/acsmaterialslett.2c00595, out.

[41] A. Bednarkiewicz, L. Marciniak, L.D. Carlos, e D. Jaque, Standardizing luminescence nanothermometry for biomedical applications, Nanoscale 12 (27) (2020) 14405–14421, https://doi.org/10.1039/D0NR03568H.

[42] S. Zhao, J. Zou, H. Xu, Q. Hu, Q. Han, e W. Wu, Luminescent enhancement and multi-mode optical thermometry of erbium doped halide Cs2(Na/Ag)BiCl6 microcrystals, J. Rare Earths 42 (11) (nov. 2024) 2018–2026, https://doi.org/10.1016/j.jre.2024.01.017.

[43] J.I. Eldridge, Luminescence decay-based Y2O3:Er phosphor thermometry: temperature sensitivity governed by multiphonon emission with an effective phonon energy transition, J. Lumin. 214 (2019) 116535, https://doi.org/10.1016/j.jlumin.2019.116535 out.

[44] R. Wei, F. Lu, L. Wang, F. Hu, X. Tian, e H. Guo, Splendid four-mode optical thermometry design based on thermochromic $Cs_3GdGe_3O_9$:Er^{3+} phosphors, J. Mater. Chem. C 10 (25) (2022) 9492–9498, https://doi.org/10.1039/D2TC01812H.

[45] S.M. Ehtesham Raza, et al., Improved thermometry via luminescence lifetime ratio of Er^{3+} and Tm^{3+} operated in the biological window, Opt. Express 32 (20) (2024) 35822, https://doi.org/10.1364/OE.534968 set.

[46] R.M. Romão, Termometria óptica baseada em vidros fosfatos dopados com érbio, Dissertação, Universidade Federal de Alagoas, Maceió (2011) [Online]. Disponível em: http://www.repositorio.ufal.br/handle/riufal/4740.

[47] S. Li, et al., Luminescence properties of $Ba_4Yb_3F_{17}$:Er^{3+} nanocrystals embedded in glass ceramics for optical thermometry, RSC Adv. 11 (37) (2021) 22798–22804, https://doi.org/10.1039/D1RA04038C.

[48] N. Rakov, F. Matias, e G.S. Maciel, UV LED-pumped Er3+-doped YOF ceramic powder: optical thermometry based on the green fluorescence, J. Lumin. 281 (jun. 2025) 121198, https://doi.org/10.1016/j.jlumin.2025.121198.

[49] P. Du, e J.S. Yu, Doping concentration-independent optical thermometric properties in Stark sublevels-based Er3+-activated BaGd2O4 luminescent thermometers, J. Lumin. 203 (nov. 2018) 172–178, https://doi.org/10.1016/j.jlumin.2018.06.028.

[50] W. Ran, et al., Er^{3+} -Activated $NaLaMgWO_6$ double perovskite phosphors and their bifunctional application in solid-state lighting and non-contact optical thermometry, Dalton Trans. 48 (13) (2019) 4405–4412, https://doi.org/10.1039/C9DT00315K.

[51] Y. Hua, e J.S. Yu, Strong green emission of Erbium(III)-Activated La_2MgTiO_6 phosphors for solid-state lighting and optical temperature sensors, ACS Sustainable Chem. Eng. 9 (14) (2021) 5105–5115, https://doi.org/10.1021/acssuschemeng.0c09375, abr.

[52] X. Li, J. Cao, F. Hu, R. Wei, e H. Guo, Transparent $Na_5Gd_9F_{32}$:Er^{3+} glass-ceramics: enhanced up-conversion luminescence and applications in optical temperature

sensors, RSC Adv. 7 (56) (2017) 35147–35153, https://doi.org/10.1039/C7RA06520E.
[53] Q. Wang, M. Liao, Q. Lin, M. Xiong, Z. Mu, e F. Wu, A review on fluorescence intensity ratio thermometer based on rare-earth and transition metal ions doped inorganic luminescent materials, J. Alloys Compd. 850 (jan. 2021) 156744, https://doi.org/10.1016/j.jallcom.2020.156744.
[54] B.M. Cruz, et al., One-step synthesis of YF3:Nd rod-like particles for contactless luminescent thermometers, Opt. Mater. 131 (2022) 112661, https://doi.org/10.1016/j.optmat.2022.112661 set.